14th International Symposium on Turbulence and Shear Flow Phenomena (TSFP14)
Heidelberg, Germany, July 28–31, 2026

ON THE K-ROUGHNESS REGIME OF STREAMWISE-ALIGNED STRUCTURED SURFACES

Stefano Cipelli, Bettina Frohnapfel, Davide Gatti
Institute of Fluid Mechanics (ISTM)
Karlsruhe Institute of Technology
Kaiserstraße 10, 76131, Karlsruhe, Germany
stefano.cipelli@kit.edu

ABSTRACT

We perform direct numerical simulations of turbulent channel flow over walls patterned with large riblets to investigate riblet behaviour in the drag-increasing regime and to validate the experimental findings of von Deyn *et al.* (2022). While riblets do not generate pressure drag and are therefore not expected to behave as canonical roughness, the physical mechanisms that govern the fully-rough regime of riblets and ultimately trigger its breakdown remain unclear. In this work we aim to characterize the mechanisms shared between the fully-rough regime of canonical rough surfaces and that of riblets. Furthermore, we seek to understand the physical mechanisms that lead, in the case of streamwise-aligned surfaces, to the breakdown of this regime, as well as to quantify the viscous size at which the breakdown occurs for different cross-section shapes.

INTRODUCTION

In wall turbulence, the fully-rough regime denotes the flow condition over canonical rough surfaces in which viscous effects no longer influence drag. In this regime the friction coefficient depends only on the physical size of the roughness elements compared to the outer scale of the flow. For this reason, the roughness function ΔU^+, which measures the drag increase relative to a smooth surface through the vertical shift in the mean velocity profile between the smooth and rough walls, increases logarithmically in this regime (Jiménez, 2004). Viscous drag is no longer the main contributor to total drag, as form drag becomes dominant, arising primarily from flow separation within the valleys between roughness elements.

Interestingly, riblets also feature this regime (Bechert *et al.*, 1997), despite being aligned with the streamwise direction and therefore lacking the pressure drag that normally dominates the drag of canonical fully-rough surfaces. Numerical experiments by Endrikat *et al.* (2021) and laboratory measurements by Gatti *et al.* (2020) and Rowin *et al.* (2025) confirm this behaviour.

The study of von Deyn *et al.* (2022) is unique in reporting that the fully-rough regime of riblets is not indefinitely sustained: while many of their tested geometries do exhibit fully-rough scaling over part of their viscous-size range, all of them eventually depart from that regime beyond a certain, shape-dependent, viscous size. After this departure the riblet roughness function ΔU^+ exhibits a peak and then becomes independent of the riblet viscous size, indicating a friction behaviour more akin to that of a smooth wall than to a canonical fully-rough surface.

Although it seems plausible that riblets should not behave as canonical rough surfaces, a limitation of von Deyn *et al.* (2022) is that they measured only pressure drop; their estimate of ΔU^+ therefore relies on an outer-layer similarity hypothesis that may break down for very large riblet geometries.

This numerical study aims to shed light on the drag-increasing behaviour of riblets. In particular, we seek to explain why riblets follow canonical fully-rough scaling over a limited range of viscous sizes, and to identify and characterize the flow mechanisms that cause this regime to break down for streamwise-aligned geometries. An analysis of the dispersive fields and the Reynolds stresses is performed, to lay the groundwork for a physical explanation of the observed roughness-function trend, with the ultimate goal of predicting the extent of the fully-rough regime of ribbed surfaces from their cross-section shape alone.

METHOD

We perform direct numerical simulations of turbulent channel flows with riblets on both walls, with the flow forced through a constant pressure gradient (CPG). The code uses second-order finite differences on a Cartesian grid, with an immersed boundary method (IBM) to represent the geometry (Luchini *et al.*, 2025). The IBM is further modified to account for the steady Stokes solution in the proximity of sharp corners, instead of the standard linear extrapolation, to make the simulations more affordable (Gatti *et al.*, 2023) in terms of grid resolution at the tips, and without compromising accuracy. Time advancement is explicit, performed using a fractional step method on a third-order Runge-Kutta scheme, where the Poisson equation for pressure is solved via an iterative successive-over-relaxation algorithm applied on a Gauss-Seidel red-black iteration. The timestep is adapted to maintain a constant CFL $= 1.5$.

The channel dimensions are $(2\pi, 2, \pi)\,\delta$ in the streamwise (x), wall-normal (y) and spanwise (z) directions, where δ is the channel half-height. The riblet characteristic dimensions are $l_g/\delta = 0.053$ (◀), 0.12 (▲), 0.24 (▼), and the friction Reynolds number (Re_τ) is varied between the values of 200 and 833 in order to obtain l_g^+ values ranging between 20 and 200. The friction velocity (u_τ) is calculated based on the total shear stress (τ_w) value at the coordinate $y = 0$, which is positioned in the domain at a distance of the longitudinal protrusion height (Luchini *et al.*, 1991) below the riblet tips, as $u_\tau = (\tau_w/\rho)^{0.5}$, where ρ is the fluid density. This configura-

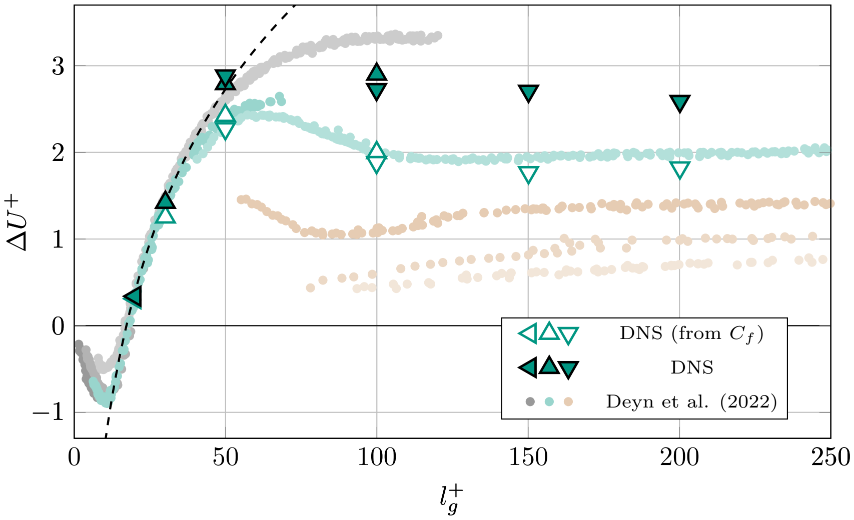

Figure 1. Ridges roughness function. Round markers correspond to experimental data from von Deyn *et al.* (2022), in which ΔU^+ has been calculated from the friction coefficient as per Equation 1. Different colors correspond to different cross-section shapes: triangular with $\approx 60°$ tip angle (α) (●●●), trapezoidal with $\alpha \approx 60°$, $k/s \approx 0.38$ (●●), trapezoidal with $\alpha \approx 60°$, $k/s < 0.22$ (●●). Triangular markers correspond to numerical data: for white markers (◁△▽) ΔU^+ is calculated as per Equation 1, for colored markers (◀▲▼) ΔU^+ is calculated from the mean velocity profiles. Different triangles correspond to different physical riblet sizes.

tion, in which the virtual origin of turbulence is not clearly defined due to the large riblet viscous size (Ibrahim *et al.*, 2021), allows at least to maintain a constant flow rate at varying Reynolds number in the laminar flow regime. Statistics are averaged over approximately 100 large-eddy-turnover time units. The grid is uniform along the streamwise direction, stretched in the spanwise (z) direction to yield $\Delta z^+ \approx 1.0$ at the riblet crests and $\Delta z^+ \approx 3.0$ at the valleys, and with a y^+-spacing following a natural stretching function as per Pirozzoli & Orlandi (2021), with a constant spacing below the $y = 0$ coordinate. Details about the spatial discretization and simulations duration for all cases are reported in Table 1.

Table 1. Spatial discretization parameters and simulations duration for all cases. l_g^+ represents the riblets size in viscous units, while Re_τ is the friction Reynolds number. n_x, n_y and n_z represent the total number of points in the streamwise, wall-normal and spanwise directions, while t_{let} represents the simulation duration in large-eddy-turnover time units.

l_g^+	Re_τ	n_x	n_y	n_z	t_{let}
20	375	408	291	816	100.6
30	250	272	271	556	110.2
50	208	226	279	430	94.6
50	417	452	379	922	98.5
100	417	452	561	860	94.5
100	833	904	473	1860	93.8
150	625	678	417	1488	109.4
200	833	904	485	1968	86.8

RESULTS

When presenting the effects of a rough surface on friction compared to a perfectly smooth wall, the most intuitive choice is to compare the friction coefficients (C_f) of the smooth and rough cases. This approach, however, is not universal, as the friction coefficient depends on the Reynolds number and therefore any measured ΔC_f is Reynolds-number dependent. As shown by Garcia-Mayoral & Jiménez (2011) and Gatti & Quadrio (2016), a Re_τ-independent measure of friction changes is the roughness function ΔU^+, obtained from the mean velocity profiles of the smooth and rough walls in the logarithmic layer, where velocities are rescaled in viscous units. Results in terms of the riblet roughness function (ΔU^+) are presented in Figure 1. For the DNS data, ΔU^+ is computed directly as the shift between the mean velocity profiles of the ribbed and smooth channels in the logarithmic layer; the corresponding values are plotted with the filled green triangular markers (◀▲▼).

To allow a direct comparison with the experimental data from von Deyn *et al.* (2022), for which mean velocity profiles are not available, we also evaluate the DNS data in the same way as the experiment, computing ΔU^+ from the friction coefficients of the ribbed and smooth $()_{,0}$ channels at the same Re_τ through:

$$\Delta U^+ = \sqrt{\frac{2}{C_{f,0}}} \left[(1 - \Delta C_f)^{-0.5} - 1 \right]. \tag{1}$$

where $\Delta C_f = (C_f - C_{f,0})/C_{f,0}$ is the relative change in friction coefficient between the ribbed and the smooth channel at the same Re_τ. This formula is exact under the assumption of high-Reynolds-number outer-layer similarity, which is not fully satisfied for all cases considered here, but provides a consistent basis for comparison since the experimental data were processed identically. As visible in Figure 1, the open triangular markers (◁△▽) obtained in this way fall almost perfectly on the experimental curve for the same cross-section shape (●

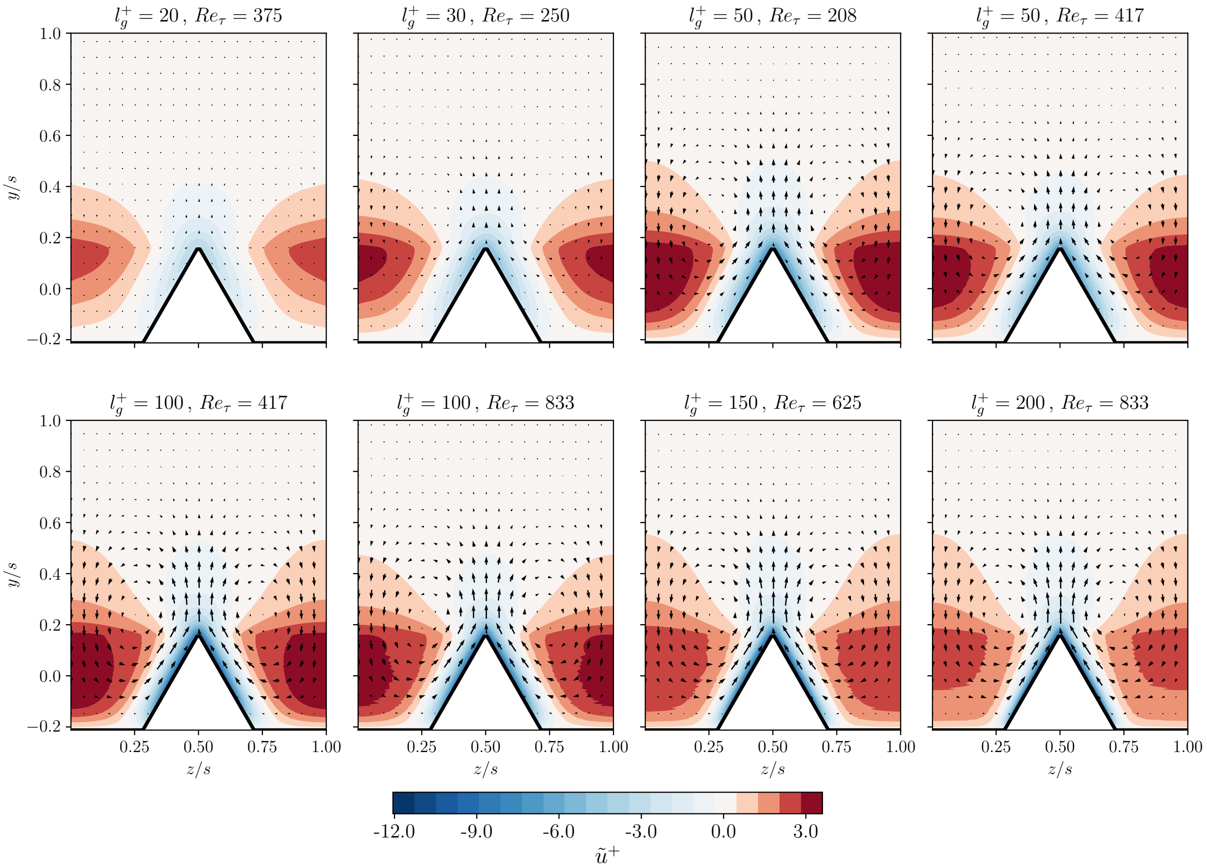

Figure 2. Wwake velocity field in the near-wall region for all simulated cases. The contour plot presents the intensity of the dispersive streamwise velocity component. The quiver plot presents the intensity and direction of the dispersive velocity field in the *yz* plane.

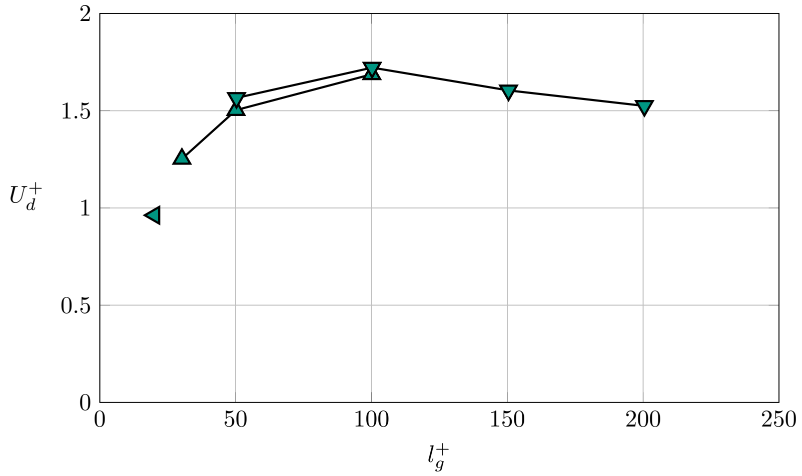

Figure 3. Intensity of the wake field U_d^+ defined as per equation (2) plotted against the riblet viscous size l_g^+.

●), thereby confirming the experimental findings.

A more robust estimate of ΔU^+ is obtained by computing the difference between the mean velocity profiles of the ribbed and smooth channels within the logarithmic layer. The values obtained from such procedure are plotted with the green triangular markers (◀ ▲ ▼) in figure 1. When evaluated in this way, cases with $l_g^+ \leq 50$ lie on the fully-rough asymptote, whereas cases with $l_g^+ > 50$ exhibit an approximately constant roughness function without a distinct peak. Taken together, the data indicate that beyond a certain viscous size these riblet geometries no longer behave as canonical roughness: their friction coefficient is again dependent on the Reynolds number. Notably, while the experimental data of von Deyn *et al.* (2022) show a distinct peak in ΔU^+ before the plateau, the present DNS results show a more gradual transition to an approximately constant value with no clear peak; this difference may stem from the outer-layer similarity assumption used to extract ΔU^+ from the experimental pressure-drop measurements, which is known to be less accurate for large riblet geometries. When considering the physical mechanisms responsible for this behaviour, it is plausible that streamwise-aligned riblets do not behave like canonical roughness: because these geometries cannot produce pressure drag, they lack the dominant mechanism that governs drag in the *k*-roughness regime. Yet it is striking that geometries with $20 \leq l_g^+ \leq 50$ nonetheless fall on the fully-rough asymptote. For canonical rough surfaces in the *k*-roughness regime, turbulence structures cannot penetrate in the roughness valleys, as it can be seen that turbulent stresses are significantly damped in favor of wake-induced stresses (Yuan & Piomelli, 2014).

In the context of turbulent channel flows with streamwise-aligned structures, which do not feature pressure drag, the only contributors to shear stress are viscous stresses, turbulent stresses and dispersive stresses (Modesti *et al.*, 2021). While the viscous (Stokes) contribution to drag is determined solely by the groove geometry and is independent of Reynolds number, the turbulent and dispersive contributions change with Re_τ and affect total drag differently. To gain better understanding of the flow features typical of riblets in this relatively unexplored drag-increasing regime, we investigate the distribution of the dispersive field and the turbulent stresses in the wall region.

On a streamwise-homogeneous (or 2D) geometry such as the present one, the dispersive velocity field $\tilde{u}_j^+$ is the deviation of the time-and-x-averaged velocity field from the mean velocity profile averaged in time and along the periodic (x, z) directions, and can be defined as follows:

$$\tilde{u}_j^+(y,z) = \langle u_j \rangle_{tx}^+(y,z) - \langle u_j \rangle_{txz}^+(y)\,, \tag{2}$$

where $\langle \cdot \rangle$ is an averaging operator, with the average taken over the dimension(s) indicated in the subscript. These fields depend on the spanwise (z) and wall-normal (y) directions, and are plotted in the near-wall region in Figure 2. The colormap indicates the streamwise dispersive component, while the quiver plot presents the components in the yz plane. The data show that the intensity and spatial extent of the dispersive field grow with the riblet viscous size up to $l_g^+ \leq 100$. For larger riblets, this contribution decreases slightly. Figure 2 also shows that dispersive fields at the same viscous size but different Reynolds number exhibit roughly the same intensity, suggesting that the dispersive field scales in viscous units.

This field can be integrated over the near-wall region up to the roughness sublayer, with δ_r as the upper bound. Here, δ_r is the wall-normal coordinate at which the spanwise derivative of the dispersive $\tilde{u}$ field falls below $u_\tau/(2s)$, where s denotes the riblet spacing. This yields an integral measure of dispersive-field intensity, U_d^+, defined as:

$$U_d^+ = \left\{ \frac{1}{L_z \delta_r} \int_0^{L_z} \int_0^{\delta_r} \tilde{u}_j^+ \tilde{u}_j^+ \, \mathrm{d}y \, \mathrm{d}z \right\}^{0.5} . \tag{3}$$

The values of U_d^+ for all cases are plotted as a function of the riblet viscous size in Figure 3. Results show that the intensity of the dispersive field increases clearly up to $l_g^+ \leq 50$, while for the largest viscous sizes U_d^+ is approximately constant, exhibiting a trend closely mirroring that of ΔU^+. In Figure 3, different markers represent different riblet physical sizes, yet results collapse well for cases sharing the same viscous size but different physical size. This occurs despite the roughness sublayer – the near-wall layer in which statistics are not homogeneous in the spanwise direction – having a different thickness for different physical riblet heights, since the roughness sublayer scales with the roughness height k (Jiménez, 2004).

Concerning the influence of turbulence on the friction behaviour of streamwise-aligned surfaces, it is known that small riblets can effectively dampen turbulence thanks to dissimilar virtual origins for the mean flow and for turbulence structures, yielding an effectively reduced channel height for turbulence (Luchini *et al.*, 1991). This is possible because the buffer layer, in which most turbulent fluctuations reside, does not interact with small riblet structures. As the riblet viscous size increases, turbulence structures begin to interact with the riblet geometry, and mixing between momentum components of different magnitudes is enhanced, increasing total drag.

In Figure 4, we present the distribution of the streamwise Reynolds stress component in the riblet region for all cases, to better visualize how the buffer layer develops around the riblet surface. For riblets small enough that turbulence does not penetrate into the grooves, the buffer layer sits above the riblet crests and its intensity is only weakly affected compared to the smooth-wall case. Consistently, for the smallest case at $l_g^+ = 20$, which lies on the fully-rough asymptote but whose grooves are still too narrow to accommodate the buffer layer, the $\overline{u'u'}^+$ component exhibits a degree of spanwise homogeneity above the crests. As the riblet viscous size increases, the spanwise inhomogeneity becomes more pronounced.

For all cases, the streamwise Reynolds stress component presents a peak close to the riblet tip, since that is the region of largest mean shear, where the wall is closest to the channel centreline. As the riblet viscous size increases, the regions of larger $\overline{u'u'}^+$ intensity migrate from above the riblet tips into the riblet grooves. Indeed, for increasingly larger viscous sizes the wall appears to be perceived as piecewise-smooth by turbulence, as the buffer-layer peak in $\overline{u'u'}^+$ follows closely the wall geometry. Other Reynolds stress components, though not shown, follow a similar trend, even if it is less pronounced due to the weaker buffer-layer peak.

A consistent picture emerges from the premultiplied 1D spectra of streamwise velocity fluctuations, shown as a function of the streamwise wavelength λ_x^+ and the wall-normal coordinate y^+ in Figure 5. These spectra provide a spanwise-averaged view of the $\overline{u'u'}$ fluctuations, together with information on the characteristic wavelengths at which structures develop and the wall-normal positions at which they occur. The wall-normal coordinate is shifted by the valley position (y_{min}^+) to permit a logarithmic representation. The thick black horizontal line marks the riblet crest position. The black contour lines represent the same contour values for the reference smooth-wall case at the same Re_τ, placed with the channel origin set either at the riblet valley or at the virtual origin of the longitudinal flow (which in the simulation domain lies at $y = 0$). Specifically, for cases at $l_g^+ \leq 50$ the smooth-wall reference is anchored at the virtual origin for the mean flow, while for cases at $l_g^+ \geq 100$ it is anchored at the riblet valley.

As the figure shows, cases lying on the fully-rough asymptote ($l_g^+ \leq 50$) exhibit a spectral peak located above the riblet crests (black horizontal line). Comparing with the smooth-wall reference, the peak for the ribbed cases is located at slightly shorter wavelengths ($\lambda_x^+ \approx 400$–500) compared to the smooth-wall case, a trend consistent with the observations of Garcia-Mayoral & Jiménez (2011).

For larger l_g^+ values, the buffer-layer spectral peak migrates into the groove; when l_g^+ becomes sufficiently

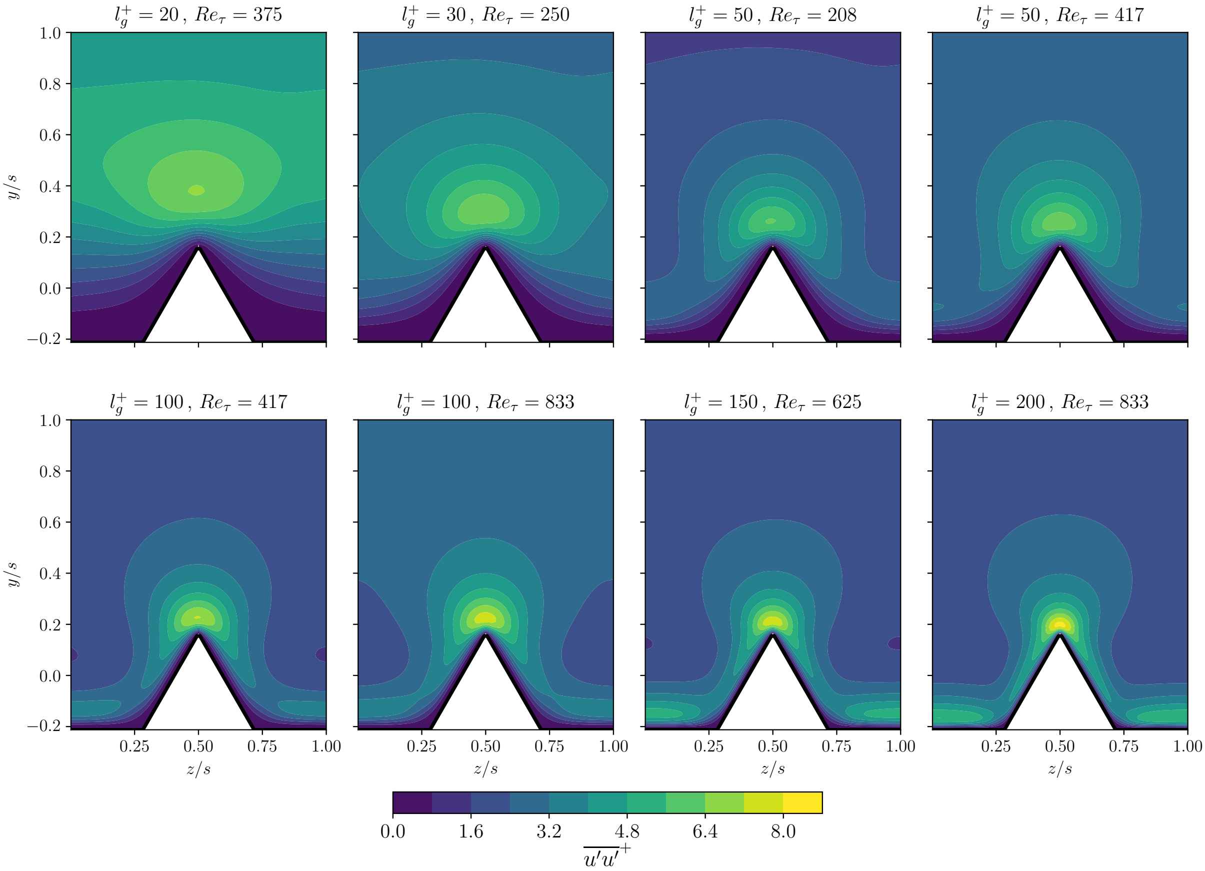

Figure 4. Distribution of the streamwise Reynolds stress component $\overline{u'u'}^+$ in the near-wall region for all simulated cases. The contour shows the spanwise and wall-normal variation of the turbulent normal stress, illustrating how the buffer-layer peak evolves with riblet viscous size and progressively moves from above the riblet crests into the grooves.

large, turbulence no longer perceives the wall as spanwise-homogeneous and the buffer layer adapts to the wall geometry, so that the surface is effectively perceived as piecewise-smooth. Interpreting the experimental data of von Deyn *et al.* (2022) in light of the present results, the k-roughness regime is seen to extend to larger l_g^+ for the triangular-riblet geometries (● ● ●), whereas the trapezoidal geometries with broader grooves (● ● ●) show no k-rough behaviour within the tested range. In other words, the experimental data suggest that groove shape strongly controls the extent of the fully-rough regime: triangular riblets, which have a high k/s ratio, tend to maintain the fully-rough scaling over a wider viscous-size interval, while riblets with a low k/s ratio depart from the k-roughness asymptote at smaller l_g^+. Testing this hypothesis numerically across different cross-section shapes is a key objective of future work. This conclusion is further supported by the experimental results of Rowin *et al.* (2025), who tested triangular riblets with large k/s and observed fully-rough behaviour up to $l_g^+ \approx 110$, the upper bound of their tested range.

CONCLUSIONS

This study clarifies the drag-increasing behaviour of streamwise-aligned structured surfaces that do not generate pressure drag. We show that, despite the absence of flow separation, the present DNS results demonstrate that these geometries follow the scaling of canonical rough surfaces over a finite range of l_g^+; beyond that range the drag increase relative to a smooth channel plateaus, in agreement with the experimental results of von Deyn *et al.* (2022). As the riblet viscous size grows, the near-wall turbulence cycle shifts from the riblet tips into the grooves. This shift is clearly visible in the premultiplied 1D spectra of the streamwise velocity component: a smooth-wall-like spectral peak appears inside the groove, originating at the groove's lowest coordinate. Future work will identify further similarities between the k-roughness behaviour of these riblet surfaces and that of canonical roughness, as well as test different riblet cross-sectional shapes. This should enable a quantitative prediction of both the characteristic viscous size at which the fully-rough regime breaks down and the asymptotic ΔU^+ value.

ACKNOWLEDGEMENTS

This work was supported by the Deutsche Forschungsgemeinschaft (DFG) under grant number 521110788. The simulations were performed on the HPE Apollo (Hawk) supercomputer at the High Performanc Computing Center Stuttgart (HLRS) under grant number 44262.

REFERENCES

Bechert, D.W., Bruse, M., Hage, W., Hoeven, J.G.T. Van Der & Hoppe, G. 1997 Experiments on drag-reducing surfaces and their optimization with an adjustable geometry. *Journal of Fluid Mechanics* **338**, 59–87.

von Deyn, Lars H., Gatti, Davide & Frohnapfel, Bettina

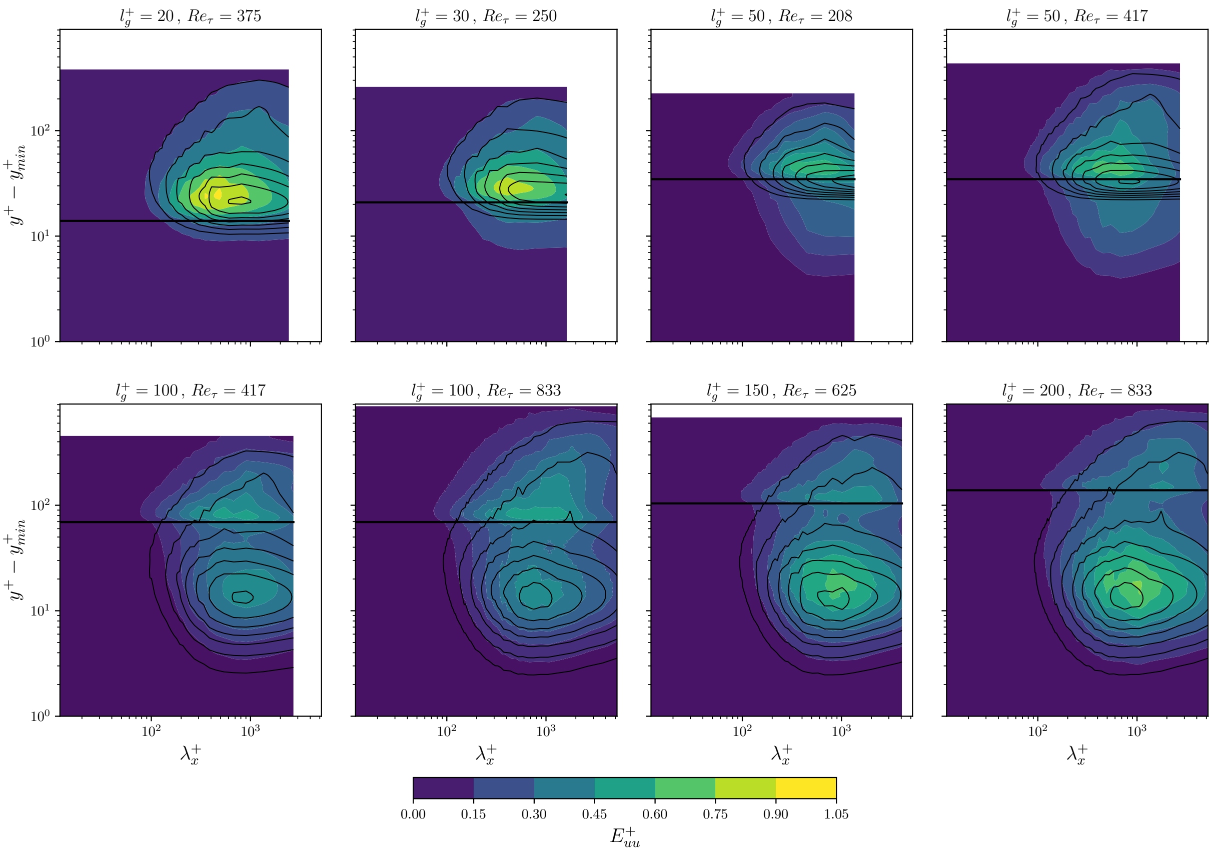

Figure 5. Premultiplied energy spectral density of the streamwise velocity component for the simulated riblet cases. The vertical axis is shifted by the position of the valley (y^+_{min}) to allow for a logarithmic scale. The thick horizontal line represents the crest position. The black lines represent the spectra of a smooth channel at the same Re_τ. To better compare the smooth channel spectra to the ribbed one, for the cases lying on the fully-rough asymptote (first row), the smooth channel wall is at $y^+ = 0$, while for the other cases at the groove valleys (y^+_{min}).

2022 From drag-reducing riblets to drag-increasing ridges. *J Fluid Mechanics* **951**, A16.

Endrikat, S., Modesti, D., MacDonald, M., García-Mayoral, R., Hutchins, N. & Chung, D. 2021 Direct Numerical Simulations of Turbulent Flow Over Various Riblet Shapes in Minimal-Span Channels. *Flow, Turbulence and Combustion* **107** (1), 1–29.

Garcia-Mayoral, R. & Jiménez, J. 2011 Hydrodynamic stability and the breakdown of the viscous regime over riblets. *Journal of Fluid Mechanics* **678**, 317–347.

Gatti, von Deyn, Forooghi & Frohnapfel 2020 Do riblets exhibit fully rough behaviour? *Experiments in Fluids* **61** (3), 81.

Gatti, D., Cipelli, S., Gattere, F., Chiarini, A., Luchini, P. & Quadrio, M. 2023 Accurate and efficient Direct Numerical SImulation of drag reduction with riblets. In *Euromech Turbulence Conference (ETC18)*. Valencia (Spain).

Gatti, D. & Quadrio, M. 2016 Reynolds-number dependence of turbulent skin-friction drag reduction induced by spanwise forcing. *Journal of Fluid Mechanics* **802**, 553–58.

Ibrahim, J. I., Gomez-de-Segura, G., Chung, D. & Garcia-Mayoral, R. 2021 The smooth-wall-like behaviour of turbulence over drag-altering surfaces: A unifying virtual-origin framework. *Journal of Fluid Mechanics* **915**, A56.

Jiménez, J. 2004 Turbulent Flows Over Rough Walls. *Annual Review of Fluid Mechanics* **36** (1), 173–196.

Luchini, P., Gatti, D., Chiarini, A., Gattere, F., Atzori, M. & Quadrio, M. 2025 A simple and efficient second-order immersed-boundary method for the incompressible Navier–Stokes equations. *Journal of Computational Physics* **539**, 114245.

Luchini, P., Manzo, F. & Pozzi, A. 1991 Resistance of a grooved surface to parallel flow and cross-flow. *Journal of Fluid Mechanics* **228**, 87–109.

Modesti, Davide, Endrikat, Sebastian, Hutchins, Nicholas & Chung, Daniel 2021 Dispersive stresses in turbulent flow over riblets. *Journal of Fluid Mechanics* **917**, A55.

Pirozzoli, S. & Orlandi, P. 2021 Natural grid stretching for DNS of wall-bounded flows. *Journal of Computational Physics* **439**, 110408.

Rowin, W. Abu, Deshpande, R., Wang, S., Kozul, M., Chung, D., Sandberg, R. D. & Hutchins, N. 2025 Experimental characterisation of Kelvin–Helmholtz rollers over riblet surfaces. *Journal of Fluid Mechanics* **1009**, A65.

Yuan, Junlin & Piomelli, Ugo 2014 Roughness effects on the Reynolds stress budgets in near-wall turbulence. *Journal of Fluid Mechanics* **760**, R1.